energies

MDPI

Article

Investigation into the Catalytic Activity of Microporous and Mesoporous Catalysts in the Pyrolysis of Waste Polyethylene and Polypropylene Mixture

Kaixin Li [1,2], Shao Wee Lee [1], Guoan Yuan [1], Junxi Lei [1], Shengxuan Lin [1], Piyarat Weerachanchai [1], Yanhui Yang [2,*] and Jing-Yuan Wang [1,*]

[1] Residues and Resource Reclamation Centre (R3C), Nanyang Environment and Water Research Institute, Nanyang Technological University, 1 Cleantech Loop, CleanTech One, Singapore 637141, Singapore; kxli@ntu.edu.sg (K.L.); leesw@ntu.edu.sg (S.W.L.); gayuan@ntu.edu.sg (G.Y.); jxlei@ntu.edu.sg (J.L.); sxlin@ntu.edu.sg (S.L.); piyarat_pw@ntu.edu.sg (P.W.)

[2] School of Chemical and Biomedical Engineering, Nanyang Technological University, Singapore 637459, Singapore

* Correspondence: yhyang@ntu.edu.sg (Y.Y.); jywang@ntu.edu.sg (J.-Y.W.); Tel.: +65-6316-8940 (Y.Y.); +65-6790-4100 (J.-Y.W.)

Academic Editor: Haolin Tang
Received: 17 February 2016; Accepted: 26 May 2016; Published: 7 June 2016

Abstract: Catalytic pyrolysis behavior of synthesized microporous catalysts (conventional Zeolite Socony Mobil–5 (C-ZSM-5), highly uniform nanocrystalline ZSM-5 (HUN-ZSM-5) and β-zeolite), Mesoporous catalysts (highly hydrothermally stable Al-MCM-41 with accessible void defects (Al-MCM-41(hhs)), Kanemite-derived folded silica (KFS-16B) and well-ordered Al-SBA-15 (Al-SBA-15(wo)) were studied with waste polyethylene (PE) and polypropylene (PP) mixture which are the main constituents in municipal solid waste. All the catalysts were characterized by Brunauer-Emmett-Teller (BET), X-ray powder diffraction (XRD), and NH3-temperature programmed desorption (TPD). The results demonstrated that microporous catalysts exhibited high yields of gas products and high selectivity for aromatics and alkene, whereas the mesoporous catalysts showed high yields of liquid products with considerable amounts of aliphatic compounds. The differences between the microporous and mesoporous catalysts could be attributed to their characteristic acidic and textural properties. A significant amount of C2–C4 gases were produced from both types of catalysts. The composition of the liquid and gas products from catalytic pyrolysis is similar to petroleum-derived fuels. In other words, products of catalytic pyrolysis of plastic waste can be potential alternatives to the petroleum-derived fuels.

Keywords: plastic recycling; catalytic pyrolysis; mesoporous catalyst; microporous catalyst; polyethylene (PE); polypropylene (PP)

1. Introduction

Plastic materials have been extensively consumed by various industry sectors including packaging, household, construction, automobile, aerospace, and electronic [1] owing to their advantageous properties, such as light weight, good strength and durability, resistance to corrosion, excellent thermal and electrical insulation, versatility and low production costs. Nevertheless, the growing consumption of plastics has resulted in an increasing amount of municipal and industrial plastic wastes generated over the decades. Non-sustainable end-of-pipe treatments such as landfill and incineration remains the most common approaches for plastic wastes management [1,2]. Landfilling non-biodegradable plastic

waste occupies precious land space [3,4]. The use of incineration can significantly reduce the need for landfill space and energy can be recovered from plastic waste. However, incineration may emit toxic air pollutants and greenhouse gases [5]. Alternative treatment of plastic waste is Pyrolysis. Pyrolysis has been gaining increasing interest over the years as a promising alternative to landfill and incineration due to its ability to recover energy from plastic wastes in the form of valuable hydrocarbons (*i.e.*, liquid hydrocarbon fuels, combustible gases and char) with low negative environmental impacts. In addition, pyrolysis is able to treat heterogeneous and contaminated polymers without pre-sorting and complex pre-treatment. The downside of this technology is the broad distribution of its product in terms of carbon number. This is due to random scission of the polymer chains during pyrolysis. Therefore, upgrading of the fuel is required before use. The introduction of the catalyst narrows the carbon distribution of the products and improves the conversion rate of the feedstock [3,5]. In addition, pyrolysis temperature and time can be lowered considerably as compared with pure thermal cracking. Several types of catalysts had been reported to be employed in catalytic pyrolysis. For instance, according to [6], Lewis acids such as aluminum trichloride and metal tetrachloroaluminate melts had been applied as homogeneous catalysts in pyrolysis of polyolefin to produce hydrocarbon gases. Ionic liquids such as 1-ethyl-3-methylimidazolium chloride-aluminum(III) chloride were also used in catalytic pyrolysis of polyethylene (PE) [7]. However, homogeneous catalysts are not popular as they are difficult to recover and separate from the liquid products [4]. In contrast, heterogeneous catalysts are considered to be more promising as they are inherently easier to recover from the products and can be readily reused [4,8]. Several studies had been conducted to examine the cracking of plastic materials over different heterogeneous solid acid catalysts, including some microporous catalysts (e.g., zeolites) [9–14] and some mesoporous catalysts (e.g., MCM-41 and SBA-15) [9,10,12–14].

Limited studies were performed on catalytic pyrolysis of waste plastics as it is challenging for traditional catalysts to convert plastic waste into fuel products of high quality. The success of the catalyst is determined by the adjustability of the acidity and its textural structure. Wide application of the modified catalyst can be achieved with an effective combination of physical structure and catalytic active compound.

This paper presents an investigation of the catalytic performance of modified microporous catalysts and macroporous catalysts in pyrolysis of plastic waste. The group of microporous catalysts consists of:

(1) Highly uniform nanocrystalline Zeolite Socony Mobil–5(HUN-ZSM-5);
(2) Conventional ZSM-5 (C-ZSM-5);
(3) β-zeolite.

While the group of mesoporous catalyst studied were:

(1) Highly hydrothermally stable Al-MCM-41 with accessible void defects (Al-MCM-41(hhs));
(2) Kanemite-derived folded silica (KFS-16B);
(3) Well-ordered Al-SBA-15 (Al-SBA-15(wo)).

Out of these six catalysts, HUN-ZSM-5, Al-MCM-41(hhs), and Al-SBA-15(wo) were modified to tailor their textural and acidic properties. Catalytic pyrolysis of plastic waste was performed using modified catalyst while the pyrolysis with other catalysts served as controls.

The feedstock used in this experiment was a mixture PE and polypropylene (PP), which have been known as the main constituents in municipal waste plastics (the mixture of PE and PP accounts for approximately 70% of the plastics). The ratio of PE and PP is 6:5 which resembles the composition of real plastic waste coming from packing and packaging applications.

The mixture of the feedstock is prepared and characterized by thermogravimetric (TG) analysis while the catalysts were characterized by Brunauer-Emmett-Teller (BET) analysis, X-ray powder diffraction (XRD) and temperature programmed desorption (TPD) of ammonia. The

liquid and gas products generated from catalytic pyrolysis of PE/PP mixture were analyzed by gas chromatography-mass spectrometry (GC-MS) and gas chromatography-thermal conductivity detector-flame ionization detector (GC-TCD-FID), respectively. The comprehensive comparisons of the catalytic performance among the six different catalysts may provide useful insights to facilitate the design of ideal catalyst for large-scale catalytic pyrolysis of plastic wastes.

2. Materials and Methods

2.1. Materials

The waste PE and PP were collected from a local plastic recycle company (Winrigo (S) Pte Ltd., Singapore) with a pellet size of 3 mm. The C-ZSM-5 used was obtained from Alfa Aesar® (Ward Hill, MA, USA). While other chemicals—Pluronic P123, cetyltrimethylammonium bromide (CTAB), tetraethylorthosilicate (TEOS), aluminum isopropoxide, tetrapropylammonium bromide, tetrapropylammonium hydroxide, phenylaminopropyltrimethoxysilane (PHAPTMS)—and other reagents used for synthesis of the other five catalysts were purchased from Sigma-Aldrich (St. Louis, MO, USA).

2.2. Catalyst Preparation and Characterization

KFS-16B and B-Zeolite were prepared according to the methods reported by Yusaku *et al.* [15] and Renzinia *et al.* [16], respectively. Al-SBA-15(wo) was synthesized using a modified synthesis route based on the method previously reported by Bhange *et al.* [17]. In the modified method, n-hexane was introduced into the impregnation step as a solvent in order to obtain a homogeneous solution. Al-MCM-41(hhs) was prepared using a method modified from the method first reported by Song *et al.* [18], which included an alkaline treatment for the raw material and a hydrothermal treatment for crystallization. HUN-ZSM-5 was prepared based on the method reported by Serrano *et al.* [19]. In this method, HUN-ZSM-5 was synthesized using high temperature pre-crystallization and the resulting zeolite seeds were functionalized by the reaction with PHAPTMS at 90 °C for 6 h. The proportion of PHAPTMS was 10 mol% with respect to the silica content in the gel. All the catalysts were tested by TG analysis to verify their effectiveness for PE/PP cracking. The cracking temperature can be decreased by 15–30 °C by applying the catalysts.

The Si/Al ratios of all the catalysts were determined to be approximately 30:1 by an inductively coupled plasma optical emission spectrometer (Optima 8300 ICP-OES, PerkinElmer, Waltham, MA, USA). Textural properties of the catalysts were determined by an ASAP 2010 nitrogen gas adsorption analyzer (Micrometrics, Norcross, GA, USA) at 77 K. Surface areas of the catalysts were estimated using the BET method. The range of P/P_0 used for BET calculations was 0.01–0.15 and 0.2–0.3 for microporous catalysts and mesoporous catalysts, respectively. Total pore volumes were measured at P/P_0 = 0.99 and the micropore volumes were determined using the t-plot method. XRD patterns of the catalysts were collected in a Ultima IV diffractometer (Rigaku, Woodlands, TX, USA) using Cu Kα radiation source (λ = 1.54056 Å) at 40 kV and 20 mA with a scan rate of 0.5 °/min. The acidity of the catalysts was measured by TPD of ammonia using an AutoChem 2920 chemisorption analyzer (Micromeritics, Norcross, GA, USA). Prior to the adsorption experiments, each sample (86–300 mg) was pre-treated with nitrogen stream in a quartz U-tube at 500 °C, followed by a temperature reduction to 100 °C. The adsorption experiments were performed by supplying the samples with small pulses of ammonia in argon gas at 100 °C until saturation. Subsequently, the samples were exposed to a flow of pure argon gas (50 mL/min) for 2 h at 100 °C to remove the reversibly and physically bound ammonia from the surface of the samples. Finally, the samples were subjected to desorption with temperature increased from 100 °C to 500 °C (heating rate: 10 °C/min) in argon stream (50 mL/min), followed by temperature holding for 15 min to ensure complete desorption of the adsorbates. The amount of ammonia desorbed within a given temperature range reflects the acid site concentration, whereas the

temperature range where most of the ammonia is desorbed indicates the acid strength of the acid sites [20,21].

2.3. Elemental Analysis of Plastic Feedstock

The metal content of plastics was measured by an inductively coupled plasma optical emission spectrometer (PerkinElmer Optima 8300 ICP-OES). The sulfur content was determined by an Elementar® CHNS Elemental Analyzer (Elementar, Hanau, Germany). The chlorine content was measured according to ASTM D808-11.

2.4. Thermogravimetric Analysis

The thermal behaviors of the plastic samples were studied using a simultaneous thermal analyzer (Netzsch STA 449 F3 Jupiter, Selb, Germany) configured for thermogravimetric analysis-differential scanning calorimeter (TGA-DSC) (Netzsch, Selb, Germany) measurements. Pure nitrogen gas (flow rate: 60 mL/min) was used to maintain an inert atmosphere within the TGA furnace and to purge the gaseous products away. In each analysis, 8–12 mg of plastic sample (ground into powder form) was loaded into the analyzer. The sample was heated to 50 °C and kept at that temperature for 2 h to remove any moisture and allow the condition within the analyzer to stabilize. The sample was then heated at a rate of 5 °C/min to a final temperature of 750 °C, and kept at that temperature for 30 min to ensure that no further weight loss would be detected. The real-time weight loss record obtained from each analysis was used to plot a derivative thermogravimetric analysis (DTG) curve. Characteristic pyrolysis temperature of each plastic sample was estimated from the DTG curves.

2.5. Pyrolysis Experiment and Analytical Techniques

The batch pyrolysis experiments were carried out in a laboratory scale installation which included an unstirred 3 dm^3 reactor and a condensation-separation apparatus (Figure 1). In each run, 10 g of plastic sample (PE/PP ratio: 6:5) was mixed with catalyst (powder form, catalyst-to-feedstock ratio is 0.03:1) in the reaction vessel and placed into the reactor. The plastic feedstock was mechanically pre-mixed with the catalyst to ensure the homogeneity before reaction. The reactor was first heated at a rate of 40 °C/min to 300 °C, followed by a temperature holding of 5 min. The temperature was subsequently increased to a final temperature of 500 °C at 10 °C/min, followed by a temperature holding of 30 min. Both the catalyst-to-feedstock ratio and the temperature program were optimized in terms of pyrolysis oil yield. The gas and oil vapor generated were purged out of the reactor by nitrogen flow (flow rate: 200 mL/min) to an oil condenser cooled by running water. The incondensable gaseous product was collected in a Tedlar® gas sampling bag to be analyzed by GC-TCD-FID afterwards. After pyrolysis, the solid residues remained in the reaction vessel, oil products collected in the oil tank, and wax products collected from the condenser and connecting pipelines were weighed. The yield of the residues (exclusive of catalyst), oil and wax were calculated as weight percentage with respect to the plastic feedstock. Gas yield was calculated by subtracting the weight percentage of residues, oil and wax products from 100%.

The composition of the oil and wax products collected was examined using a gas chromatograph (Agilent 7890B GC system, Santa Clara, CA, USA) equipped with Agilent HP-5 MS column (length: 30 m, inside diameter: 0.25 mm), coupling with a mass spectrometer (Agilent 5977A MSD). The injection volume was 1 μL and the split ratio was set to 100:1. The temperature of the injection port, quadrupole and ion source were set at 250, 150 and 230 °C, respectively. Furnace temperature was programmed at an initial temperature of 40 °C and subsequently raised in a stepwise manner (increased at 1 °C/min to 45 °C and held for 2 min, followed by temperature increase at 5 °C/min to 150 °C and holding time of 2 min, 10 °C/min to 210 °C without temperature holding, and finally a temperature increase at 20 °C/min to 280 °C and holding time of 10 min). The flow rate of helium carrier gas was set to 1.2 mL/min. Identification of different constituents of the oil and wax products was done by computer matching against the NIST11 mass spectral library (Wiley Registry™, Hoboken, NJ, USA), the peaks

representing the major constituents were further verified by comparing their mass spectrum profile of the oil and wax products with that of a calibration standard. Any library-matched species which exhibited a match quality lower than 80% was classified as "not identified" and rejected. An external method is employed in the quantitative GC analysis. The non-condensable gases collected were analyzed by a gas chromatograph (Agilent 7890B GC system) coupled with two thermal conductivity detectors (TCD) and a flame ionization detector (FID). The temperature of both the inlet and detectors (TCDs and FID) was set at 250 °C. Furnace temperature was programmed at an initial temperature of 40 °C (holding time: 1 min) and subsequently raised at 20 °C/min to 80 °C without temperature holding, followed by a temperature increase at 30 °C/min to 190 °C and holding time of 1.33 min. Helium carrier gas was supplied at flow rate of 20 mL/min and the split ratio was set to 80:1. The peaks corresponding to different gas constituents were identified and quantified by comparing their retention times and the area with those of the calibration standards. Nitrogen was excluded from the computation for the gas composition.

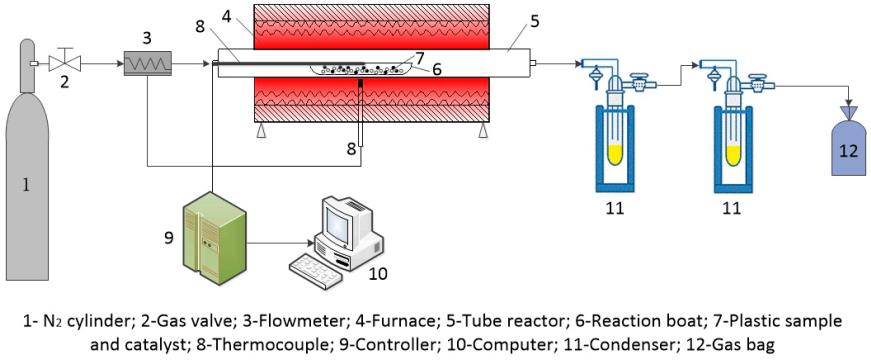

Figure 1. Schematic diagram of the experimental setup for pyrolysis.

3. Results and Discussion

3.1. Characterization of Plastic Feedstock

The characterization result of single plastic waste was presented in Table 1. Figure 2 illustrates the DTG curves of PE, PP and their combination (PE/PP ratio: 6:5). T_0 and T_f are defined as the temperature at which decomposition starts and ends, respectively, while the temperature at which the decomposition rate reaches the maximum is referred to T_{max}. The thermal decomposition of single PE and PP featured a single-step weight loss pattern with an increase in temperature, demonstrating that the thermal decomposition of single PE and PP is a single-step reaction. As shown in Figure 2, the decomposition of PE took place within the temperature range of 355–477 °C, whereas the decomposition of PP occurred at 329–467 °C. The slightly higher T_0, T_f and T_{max} of PE as compared with those of PP indicated that PE has a higher thermal stability than PP. The decomposition temperature range of PE/PP mixture was similar to that of single PE and PP. However, its DTG curve contained two partially-overlapped peaks (at 436.3 °C and 446.7 °C), suggesting that the decomposition of the mixture is a multiple-step reaction. Interestingly, the T_{max} of both peaks for PE/PP mixture did not coincide with the T_{max} of single PE and PP. Instead, they occurred at temperatures between the T_{max} of single PE and PP. Furthermore, the magnitude of the two peaks did not appear to correspond to the ratio of PE and PP in the mixture, as well as the magnitude of the peaks for single PE and PP. These imply the existence of a possible interaction between PE and PP which could alter their thermal behavior. PE and PP decomposition are radical chain mechanisms, the primary radical initiated by random scission of PP can capture the hydrogen from PE to initiate PE decomposition at lower temperature [22], which caused the impedimental effect of PP decomposition and enhancing the effect of PE decomposition in pyrolysis of PE/PP mixture. Besides, it is worth mentioning that since PE/PP

mixture was almost completely decomposed prior to reaching 500 °C, it was selected as the final pyrolysis temperature for the pyrolysis experiments presented in the later part of this paper.

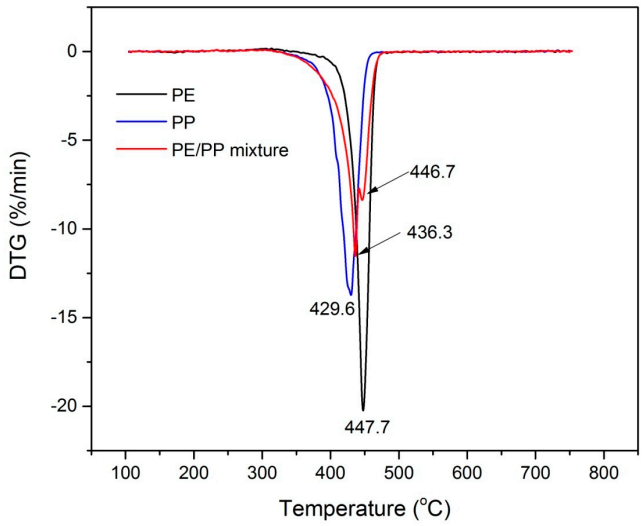

Figure 2. Derivative thermogravimetric analysis (DTG) curves of PE, PP and PE/PP mixture.

Table 1. Elemental analysis of plastic feedstock (results expressed in ppm). PE: polyethylene; PP: polypropylene; n.d.: not detected.

Plastic Feedstock	Na	Al	Fe	Mg	O	Cl	S
PE	n.d.	n.d.	n.d.	n.d.	1.68	0.04	0.35
PP	0.14	0.49	0.03	0.93	2.36	0.11	0.20

3.2. Characterization of Catalysts

Figure 3 depicts the nitrogen adsorption/desorption isotherms exhibited by the catalysts employed in this work. According to the International Union of Pure and Applied Chemistry (IUPAC) classification of adsorption isotherms, the shapes of the adsorption isotherm for C-ZSM-5, B-Zeolite and HUN-ZSM-5 (Figure 3a–c) were a combination of the type I (Langmuir) isotherm and type IV isotherm with high adsorption capacity at low relative pressures ($P/P_0 < 0.1$) and a well-defined hysteresis loop. The high adsorption volume (around 60 $cm^3 \cdot g^{-1}$) at low relative pressure ($P/P_0 < 0.1$) indicated the presence of microporous adsorption (type I) in these three catalysts. As the relative pressure increases, capillary condensation occurred, all three catalysts exhibited a type IV of isotherm, indicating the presence of small amount of larger cavities (mesopores, inter-particulate spaces) in their structures. The hysteresis loop found in the adsorption isotherm of the three catalysts, which resembles a H4 type hysteresis loop, is commonly found in solids composed of aggregates of particles with uniform size and/or shape that form narrow slit-shaped pores [23]. In addition, the steep jump at high relative pressures ($P/P_0 > 0.9$) in the isotherm of the three catalysts revealed the existence of some macropores in their structures.

Table 2 shows the textural properties of the catalysts as determined by the application of the BET, t-plot and BJH methods. Both B-Zeolite and HUN-ZSM-5 showed higher adsorption capacity than C-ZSM-5, resulting in larger BET surface areas (474.9, 617.2 and 393.9 $m^2 \cdot g^{-1}$ for B-Zeolite, HUN-ZSM-5 and C-ZSM-5, respectively) and higher total pore volumes (0.304, 0.398 and 0.258 $cm^3 \cdot g^{-1}$ for B-Zeolite, HUN-ZSM-5 and C-ZSM-5, respectively) (Table 2). While B-Zeolite and HUN-ZSM-5 exhibited a comparable adsorption capacity, the latter exhibited a larger BET surface area and a higher total pore volume owing to the smaller crystal size of HUN-ZSM-5.

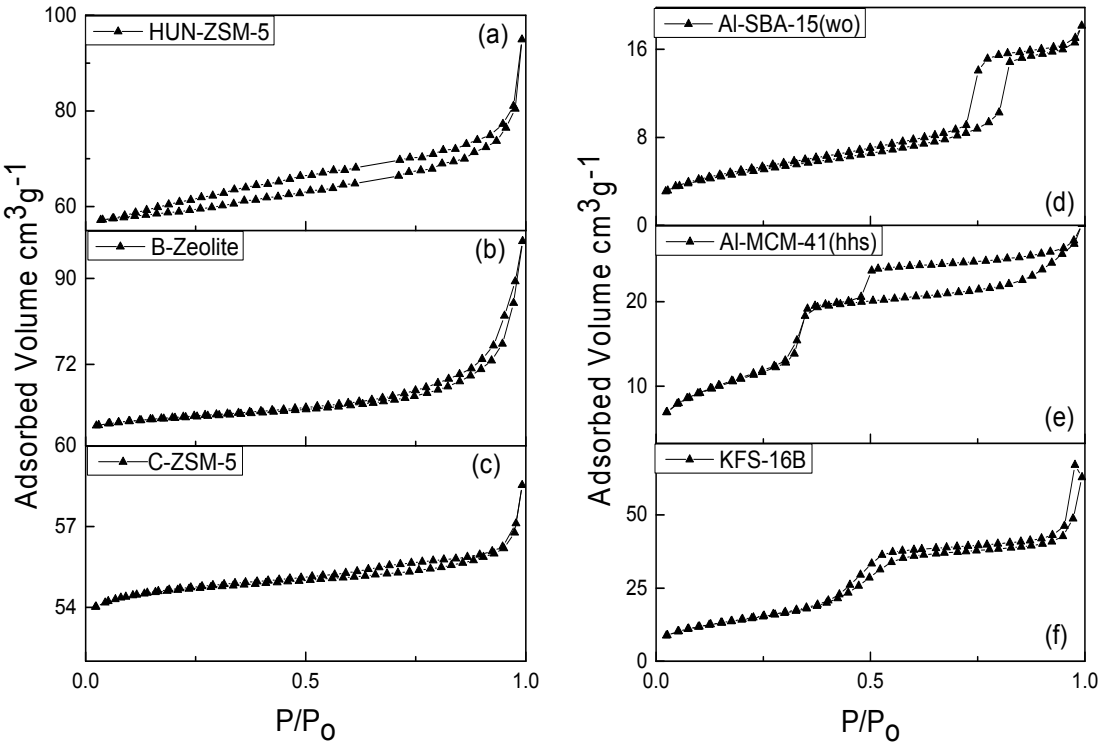

Figure 3. Nitrogen gas adsorption/desorption isotherms of the catalysts: (**a**) HUN-ZSM-5; (**b**) B-Zeolite; (**c**) C-ZSM-5; (**d**) Al-SBA-15(wo); (**e**) Al-MCM-41(hhs); and (**f**) KFS-16B.

Table 2. Textural properties and acidity of different catalysts. BET: Brunauer-Emmett-Teller; n.a.: not applicable.

Experiment	Textural Properties [1]			Acidity (mmol $NH_3 \cdot g^{-1}$)	
Catalyst	BET Surface area [2] ($m^2 \cdot g^{-1}$)	Total Pore Volume ($cm^3 \cdot g^{-1}$)	Mesopore Diameter (Å)	Weak Acid Site (100–280 °C)	Strong Acid Site (300–550 °C)
C-ZSM-5	393.9	0.258	n.a.	0.238	0.269
B-Zeolite	474.9	0.304	n.a.	0.215	0.098
HUN-ZSM-5	617.2	0.398	n.a.	0.505	n.d.
KFS-16B	866.2	1.072	45.09	0.097	0.05
Al-MCM-41(hhs)	1005	1.003	33.94	0.108	0.115
Al-SBA-15(wo)	742.1	1.106	52.74	0.049	n.d.

[1] Nitrogen adsorption at 77 K; [2] Multi-point BET method.

As illustrated in Figure 3d,f, the shapes of the adsorption isotherm for Al-MCM-41(hhs), KFS-16B, Al-SBA-15(wo) were of type IV, which is characteristic of mesoporous materials. The three catalysts also showed noticeable H4 type hysteresis loops in their isotherms. The steep jump in the adsorption isotherm of Al-SBA-15(wo) occurred at a pressure (P/P_0 = 0.77) higher than that of Al-MCM-41(hhs) (P/P_0 = 0.35) and KFS-16B (P/P_0 = 0.55), indicating that the pore size of Al-SBA-15(wo) is the largest among the three mesoporous catalysts. This is further demonstrated by their respective mesopore diameters listed in Table 2. The pore diameters of these three catalysts were found to be in agreement with the typical pore size of a mesoporous material (around 2–50 nm). Compared with the microporous catalysts, the total pore volume of all the three mesoporous catalysts were significantly larger, indicating the existence of relatively high internal porosity in the mesoporous catalysts. Besides, the mesopore diameter and total pore volume of the three mesoporous catalysts were shown to increase in the following order: Al-MCM-41(hhs) < KFS-16B < Al-SBA-15(wo). Conversely, the BET surface area of the three catalysts increased in the reverse order (Al-SBA-15(wo) < KFS-16B < Al-MCM-41(hhs)) as

a result of an increasing amount of mesopores being incorporated into the structure. As compared with the non-hydrothermal preparation method for KFS-16B, the introduction of the hydrothermal treatment to the preparation of Al-MCM-41(hhs) may facilitate the formation of mesopores in the catalyst's structure, resulting in a higher BET surface area.

The XRD patterns for the microporous catalysts and mesoporous catalysts are shown in Figure 4a,b, respectively. It can be seen from Figure 4a that XRD patterns of all the microporous catalysts exhibited two clusters of characteristic peaks for the MFI structure (one cluster in the range of 5°–10° and the other in the range of 20°–30°). These diffraction peaks associated with the MFI structure were sharp and distinct, indicating that they are all single-phase zeolites with a highly ordered micropore structure. Close inspection of the diffraction patterns between 20° and 30° revealed that the cluster of peaks for HUN-ZSM-5 was broader and of higher intensity as compared with the other two microporous catalysts. This could be attributed to the introduction of high temperature pre-crystallization and PHAPTMS to the synthesis of HUN-ZSM-5. The XRD pattern of HUN-ZSM-5 depicted in Figure 4a is similar to the results reported by Serrano *et al.* [24], who had used a similar method for pre-crystallization and functionalization of zeolite seeds.

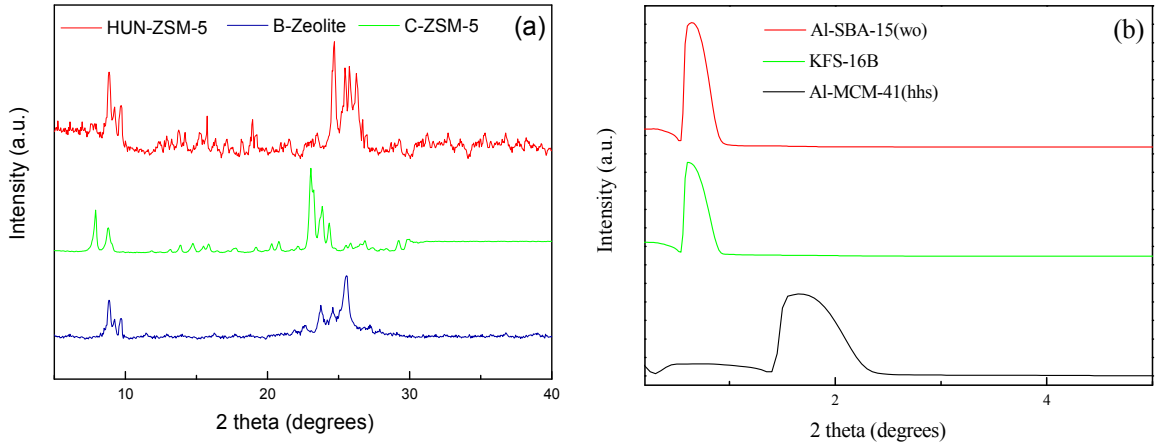

Figure 4. X-ray powder diffraction (XRD) patterns of the six catalysts: (**a**) HUN-ZSM-5, B-Zeolite and C-ZSM-5; and (**b**) Al-SBA-15(wo), KFS-16B and Al-MCM-41(hhs).

The diffractograms of Al-MCM-41(hhs), KFS-16B and Al-SBA-15(wo) presented the main diffraction peak (100 reflection) at 2θ of 1.9°, 0.9° and 1.0°, respectively. All the peaks were well-resolved, sharp and distinct, implying good crystallinity of these catalysts. The diffraction peak (100 reflection) of Al-MCM-41(hhs) was broader and of slightly lower intensity than that of KFS-16B and Al-SBA-15(wo), probably due to the effect of hydrothermal treatment introduced to the preparation for Al-MCM-41(hhs). The absence of two other characteristic peaks (110 reflection and 200 reflection) in the XRD spectra of all three mesoporous catalysts reflected a relatively low degree of mesoscopic hexagonal ordering in the structure of the catalysts [25]. The results are in agreement with the observations reported by Aguado *et al.* [26], which showed that the incorporation of aluminum into a siliceous material could perturb the hexagonal ordering of the pores to some extent, giving rise to a wormhole-like structure with a slightly irregular pore arrangement. However, such distorted pore architecture did not appear to have a significant detrimental effect on the catalytic behavior of the mesoporous catalysts, as evidenced by the pyrolysis studies conducted by Liu *et al.* [27].

The acidity of the six catalysts as determined by TPD of ammonia is presented in Table 2. In general, the microporous zeolitic catalysts exhibited stronger acid properties than the mesoporous catalysts synthesized in this work. Among all six catalysts, C-ZSM-5 showed the greatest acidity with high abundance of both weak acid site (0.238 mmol $NH_3 \cdot g^{-1}$ desorbed at 100–280 °C) and strong acid site (0.269 mmol $NH_3 \cdot g^{-1}$ desorbed at 300–550 °C). The presence of both weak and strong acid sites in

C-ZSM-5 is consistent with the observations reported by Hernández *et al.* [28] and Elordi *et al.* [29]. According to the pyridine chemisorption and infrared spectroscopic studies reported by González-González-Velasco *et al.* [30], the strong acid site, which were identified by NH_3 desorption at a higher temperature in our case, most likely represented the Brønsted acid sites. While B-Zeolite also contained two types of acid sites with a weak acid site concentration (0.215 mmol $NH_3 \cdot g^{-1}$ comparable to that of C-ZSM-5, its content of strong acid sites was found to be much lower (0.098 mmol $NH_3 \cdot g^{-1}$). Besides, no strong acid site was detected in HUN-ZSM-5. Nevertheless, HUN-ZSM-5 showed significantly high abundance of weak acid sites (0.505 mmol $NH_3 \cdot g^{-1}$), giving it a total acidity comparable to that of C-ZSM-5, in spite of the absence of strong acid sites. The high acidity may be attributed to the small crystal size of HUN-ZSM-5 which facilitates the diffusion of ammonia out of the catalyst during the desorption process [31].

Among the three mesoporous catalysts, Al-MCM-41(hhs) showed the highest acidity, with a relatively high amount of weak and strong acid sites (0.108 mmol $NH_3 \cdot g^{-1}$ and 0.115 mmol $NH_3 \cdot g^{-1}$, respectively). While KFS-16B was found to contain a similar amount of weak acid sites (0.097 mmol $NH_3 \cdot g^{-1}$), it exhibited lower total acidity than Al-MCM-41(hhs), owing to its lower content of strong acid sites (0.05 mmol $NH_3 \cdot g^{-1}$). The higher acidity of Al-MCM-41(hhs) compared with KFS-16B could be attributed to the introduction of a hydrothermal method into the catalyst preparation process, which promotes the BET surface area of the catalyst, allowing greater accessibility of NH_3 to the strong acid centers dispersed on the pore wall of the catalyst. Al-SBA-15(wo) exhibited the weakest acid properties among the six catalysts both in terms of the acid strength and the amount of acid sites, as denoted by its lack of a strong acid site and weak acid sites (0.049 mmol $NH_3 \cdot g^{-1}$), as well as the lowest T (150 °C, this value was obtained by NH_3-TPD and not shown here) indicative of the acid strength among the six catalysts.

3.3. Catalytic Pyrolysis

3.3.1. Pyrolysis Yields

The yields (in wt%) of solid residue, gaseous products, as well as oil and wax obtained from the catalytic pyrolysis of PE/PP mixture over different catalysts are presented in Figure 5. The results from non-catalytic thermal decomposition are also presented for comparison. As shown in the figure, all the seven pyrolysis runs produced only negligible amounts of solid residue, indicating a high conversion of the plastic feedstock in all pyrolysis experiments. All catalysts synthesized in this work, except Al-SBA-15(wo), manifested strong cracking activities in the pyrolysis of PE/PP mixture, as evidenced by the significantly reduced yields of liquid and wax product and the improved gas yields in comparison to the non-catalytic thermal decomposition. In general, the microporous catalysts showed higher gas yields and lower oil and wax yields as compared with their mesoporous counterparts, probably due to the highly acidic nature of the zeolitic catalysts that often results in severe secondary cracking of the primary pyrolytic intermediate species. Besides that, the size selectivity of the catalysts could also contribute to the high gas yield associated with the microporous catalysts.

Among the three microporous catalysts, C-ZSM-5 exhibited the strongest cracking activity, as denoted by the highest gas yield (57.7%) and the lowest oil and wax yield (41.5%). A similar catalytic performance was also observed in the case of B-Zeolite. Despite having the largest BET surface area among the microporous catalysts and a total acidity comparable to that of C-ZSM-5, HUN-ZSM-5 showed a milder cracking activity (gas yield: 38.9%) than the other two microporous catalysts. This could be attributed to the absence of strong acid sites in HUN-ZSM-5, therefore implying that the strong acid sites (most likely the Brønsted acid sites), rather than the weak acid sites, may play a more predominant role in the secondary cracking of hydrocarbons catalyzed by the zeolitic catalysts. Besides, it is worth noting that the cracking activities associated with the zeolitic catalysts observed in this study are in agreement with the findings reported by several other groups [23,28,32,33].

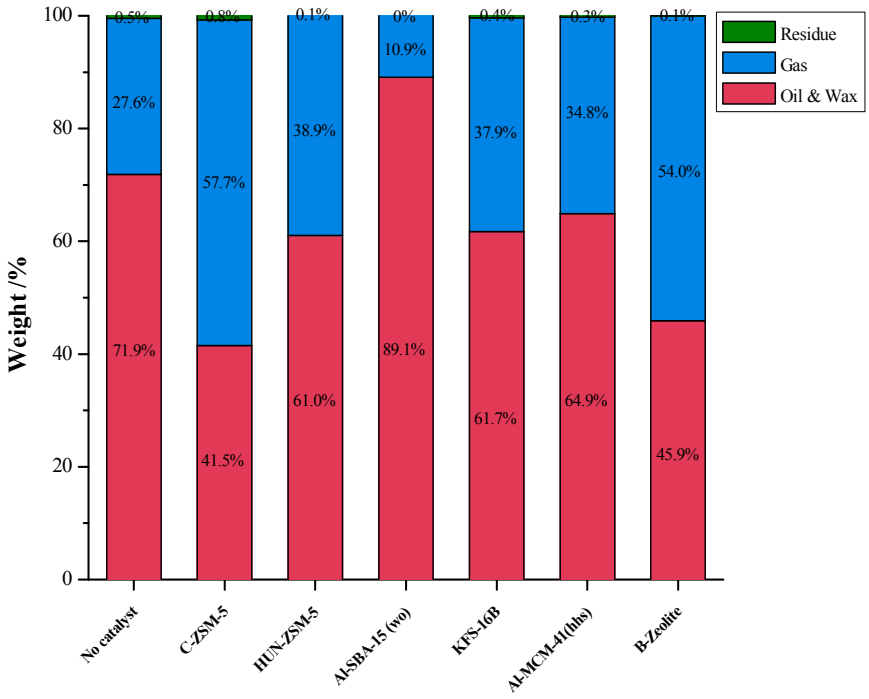

Figure 5. Pyrolysis yields of the catalytic pyrolysis of PE/PP mixture over different catalysts.

Among the six catalysts, Al-SBA-15(wo) showed the weakest cracking activity, as evidenced by the highest oil and wax yield (89.1%) and the lowest gas yield (10.9%). In fact, the cracking reactions associated with Al-SBA-15(wo) were even milder than the non-catalytic thermal degradation. This suggests that the mild cracking ability associated with Al-SBA-15(wo) favor the production of oil and wax. On the contrary, relatively low oil and wax yields were obtained over KFS-16B and Al-MCM-41(hhs) (61.7% and 64.9%, respectively). The lower oil and wax yields observed as compared with that of Al-SBA-15(wo) were probably due to differences in textural properties and acidity. The pyrolysis with KFS-16B and Al-MCM-41(hhs) shared a similar product yield despite the fact that Al-MCM-41(hhs) possessed a higher BET surface area and greater amount of strong acid sites. This indicated that the stronger cracking activities associated with KFS-16B and Al-MCM-41(hhs) could be mainly attributed to their relatively high number of weak acid sites as compared with that of Al-SBA-15(wo). In contrast, the influence of high BET surface area of these catalysts on the cracking reactions appeared to be less significant in the pyrolysis of PE/PP mixture. The prominent role of catalyst's acidity observed in our studies is somewhat consistent with the findings reported by Liu *et al.* [27]. Through studying the catalytic performance of different types of MCM-41 in co-pyrolysis of PE and pubescens, they concluded that the catalysts' acidity, rather than the surface area, plays a more significant role in the cracking of primary pyrolytic intermediates.

3.3.2. Analysis of Pyrolysis Oil and Wax

The qualitative and quantitative analyses of the liquid and wax products by GC-MS are presented in Figure 6 and Table 3. Figure 6 shows the carbon number distribution of the liquid and wax products, while the main constituents of the products and their respective percentage contents are listed in Table 3.

As shown Figure 6, the pyrolysis liquid and wax product obtained from thermal decomposition was a mixture of C_6–C_{40} compounds, in which the content of C_6–C_{12} fraction and C_{13}–C_{20} fraction were similar, giving a relatively even carbon number distribution across different fractions as compared with that of the products obtained from catalytic pyrolysis. The high variability of the liquid and wax product in terms of the molecular weight of all the constituents was due to the random scission of

the polymer chains under the sole effect of temperature. Since most engines operate only on fuels with a fairly narrow carbon number range, the fuel products generated from thermal decomposition of plastics cannot be readily used and require further upgrading treatment. On the other hand, the microporous catalysts produced a carbon number distribution which is skewed towards the smaller carbon numbers (C_6–C_{12} fraction). The results are in good agreement with the high yields of light, gaseous hydrocarbons shown in Figure 5, further confirming the strong cracking activities associated with the microporous catalysts. As shown in Figure 6, HUN-ZSM-5 exhibited an exceptionally high selectivity for the C_6–C_{12} fraction and low yields of the heavier oil fractions (*i.e.*, C_{13}–C_{20} and C_{21}–C_{40}). B-Zeolite also showed considerably high yield of light compounds in the range of C_6–C_{12}. Combining the results illustrated in Figure 5 and Figure 6, HUN-ZSM-5 displayed advantages over B-Zeolite and C-ZSM-5 in terms of yield and quality of liquid products. Since the liquid hydrocarbons in the range of C_6–C_{12} is representative of gasoline, this modified zeolite catalyst has shown great potential to be applied in industry for gasoline production from plastic wastes.

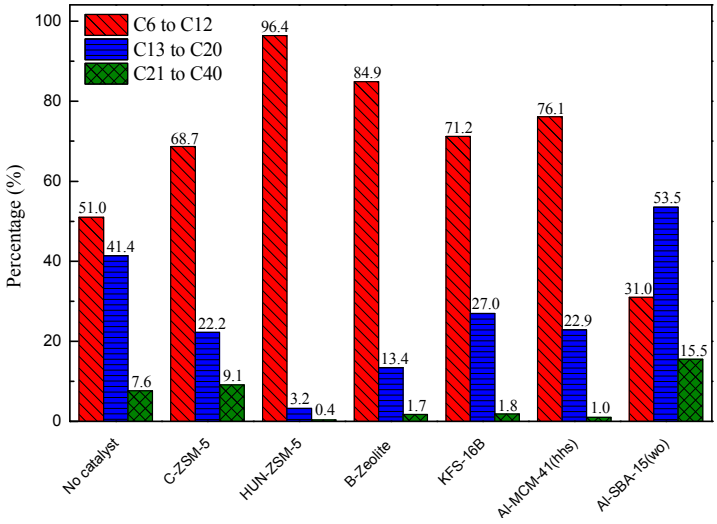

Figure 6. Distribution of the liquid and wax products in terms of carbon number.

Table 3. Main constituents of the pyrolysis oil and wax products determined by gas chromatography-mass spectrometry (GC-MS) (%area).

Experiment	Light Hydrocarbons ($\leqslant C_{13}$)				Heavy Hydrocarbons ($>C_{13}$)			
Catalyst	Alkane	Alkene	Cycloparaffin	Aromatics	Alkane	Alkene	Cycloparaffin	Aromatics
No catalyst	9.5	22.3	7.1	1.5	27.2	20.7	0.8	n.d.
C-ZSM-5	13.0	16.9	13.4	42.8	12.4	n.d.	n.d.	n.d.
HUN-ZSM-5	0.7	78.4	9.1	7.2	n.d.	n.d.	n.d.	n.d.
B-Zeolite	7.0	47.3	15.1	13.2	7.1	4.3	n.d.	n.d.
KFS-16B	7.3	46.2	6.0	1.0	10.6	17.4	n.d.	n.d.
Al-MCM-41(hhs)	5.5	59.7	9.8	n.d.	16.0	4.2	n.d.	n.d.
Al-SBA-15(wo)	6.3	11.4	5.6	n.d.	37.2	18.0	0.9	n.d.

Among the mesoporous catalysts, KFS-16B and Al-MCM-41(hhs) shared a similar carbon number distribution pattern which revealed a good selectivity for the light hydrocarbon fraction, in particular the C_6–C_{12} fraction. The skewed carbon number distribution associated with KFS-16B and Al-MCM-41(hhs) observed in our studies is consistent with several studies reported previously [34,35]. On the other hand, Al-SBA-15(wo) appeared to have good selectivity for the C_{13}–C_{20} fraction, which is the fraction representative of diesel in terms of carbon numbers. Although the oil product produced by Al-SBA-15(wo) was of a lower quality as a result of its relatively even carbon number distribution, the catalyst can still be a potential catalyst candidate for diesel production from plastic materials owing to

the high oil yield attainable with this catalyst (as shown in Figure 5). Besides, the disadvantage of Al-SBA-15(wo) arising from the relatively even carbon number distribution can be, to some extent, offset by the use of appropriate distillation and fuel-upgrading treatment following the pyrolysis process.

As shown in Table 3, a large amount of aliphatic, aromatic and cyclic compounds was observed in the light hydrocarbon fractions ($\leqslant C_{13}$) while the heavy hydrocarbon fractions (C_{13}–C_{20}) were mainly composed of aliphatic compounds.

Among the three zeolitic catalysts, C-ZSM-5 exerts the strongest aromatization activity, with the aromatic compounds constituting as much as 42.8% of the oil and wax product. The high aromatization activity of C-ZSM-5 in the pyrolysis of plastic materials had been demonstrated by other research groups [23,36]. The strong aromatization activities of zeolite could be largely attributed to the Brønsted acid sites (*i.e.*, the strong acid sites) dispersed in its structure, where aromatization reactions are favored [37,38]. This explains the relatively low aromatics yield observed in the cases of B-Zeolite and HUN-ZSM-5, as these catalysts contain a relatively low number of Brønsted acid sites (Table 2). Among the six catalysts, both B-Zeolite and HUN-ZSM-5 showed high selectivity for alkene. Modified catalyst HUN-ZSM-5 displayed outstanding selectivity of alkene compounds of 78.4%. This was probably due to the nano-crystallinity of HUN-ZSM-5 which favored the formation of alkene.

As compared with microporous catalysts, the mesoporous catalysts produced considerably low quantities of aromatic compounds, indicating that aromatization was not favoured by these catalysts. Instead, significant amounts of aliphatic compounds (including alkane and alkene) were observed in the light hydrocarbon fraction, especially in the cases of Al-MCM-41(hhs) and KFS-16B. The result is different from the findings of Liu *et al.* [27] which demonstrated a strong aromatization effect of Al-MCM-41 on the intermediate species in the pyrolysis of LDPE. The difference may be attributed to the different contact modes between the catalyst and plastic feedstock employed in the pyrolysis experiments (liquid contact was employed in our case while vapor contact was used in the study of [27]), which could possibly affect the catalytic activities of the catalyst. The oil and wax product obtained by Al-SBA-15(wo) consisted of a large amount of aliphatic compounds, particularly in the heavy hydrocarbon fractions (37.2% of alkane and 18.0% of alkene). It is also worth mentioning that Al-SBA-15(wo) exhibited a high selectivity for eicosane (the result now shown here), which is one of the representative hydrocarbons in diesel fuel, further showing the good potential of this catalyst in the production of valuable diesel products from the pyrolysis of plastic materials.

3.3.3. Analysis of Pyrolysis Gas

The composition of gas products generated from thermal decomposition and catalytic pyrolysis is presented in Table 4. The pyrolysis gases were essentially composed of H_2 and a series of hydrocarbons with the carbon number ranging from C_1 to C_5. The pyrolysis gas generated from thermal decomposition was characterized by a mixture of C_1–C_5 gas, in which the content of C_1–C_4 gases was comparable. With the introduction of the microporous zeolitic catalysts, the amount of H_2 content increased drastically. The H_2 in the pyrolysis gas was probably a by-product of the aromatization reactions catalyzed by the microporous catalysts. With reference to Table 3 and Table 4, use of microporous zeolitic catalysts increases the amount of H_2 generated with increasing amounts of aromatics. In addition, the three microporous catalysts generally exhibited high selectivity for C_3H_6 and C_4H_8. This could be mainly attributed to the shape selectivity of this type of catalyst. The high selectivity for the C_3–C_4 products associated with the zeolite catalysts is consistent with the results previously reported by Wei *et al.* [39]. Among the catalysts synthesized in this work, C-ZSM-5 showed the highest C_3H_6 yield (45.6%), possibly resulting from the pore architecture of C-ZSM-5 that favors the production of C_3H_6 in pyrolysis of PE/PP mixture.

Table 4. Composition of the pyrolysis gas products (mol%).

Catalyst	H_2	CH_4	C_2H_4	C_2H_6	C_3H_6	C_3H_8	C_4H_8	C_4H_{10}	C_5H_{10}	C_5H_{12}
No catalyst	n.d.	12.0	12.1	17.2	23.5	8.0	22.8	3.7	n.d.	0.7
C-ZSM-5	10.0	1.4	1.9	1.9	45.9	9.0	21.1	6.5	0.7	0.8
B-Zeolite	2.5	1.6	1.7	1.1	32.2	2.0	38.6	8.6	5.1	1.3
HUN-ZSM-5	6.1	2.3	1.7	2.1	25.8	3.3	24.0	12.3	4.2	4.7
KFS-16B	7.4	7.6	5.4	7.1	27.5	5.5	23.3	5.3	3.9	2.3
Al-MCM-41(hhs)	5.3	0.8	1.0	0.4	33.9	1.0	29.0	2.3	6.3	0.9
Al-SBA-15(wo)	5.1	18.8	17.6	14.4	21.0	6.8	7.9	2.1	1.7	1.6

The effects of the mesoporous catalysts on the composition of pyrolysis gas were also significant. The production of C_3H_6 and C_4H_8 was also noticeable in the case of KFS-16B and Al-MCM-41(hhs). In contrast to the other five catalysts, the carbon number distribution of the gaseous hydrocarbon products produced by Al-SBA-15(wo) was relatively even. On the other hand, it should be noted that the formation of H_2 in the pyrolysis over the mesoporous catalysts was not in line with the content of aromatics, which is in contrast to the case of microporous catalysts. It is reported that the formation of hydrogen attributed not only to the aromatization in the pyrolysis process, but also to the dehydrogenation of polymer-derived radicals generated from the primary cracking reactions [27].

Finally, it is worth noting that the composition of pyrolysis gas products obtained with all six catalysts appeared to be similar to that of liquid petroleum gas. Hence, the pyrolysis gas generated from catalytic pyrolysis of plastic materials may be considered a potential alternative to the conventional fuel gas to alleviate the growing energy demand in the industry.

4. Conclusions

Three microporous catalysts (C-ZSM-5, HUN-ZSM-5, and B-Zeolite) and three mesoporous catalysts (Al-MCM-41(hhs), KFS-16B, and Al-SBA-15(wo)) were synthesized, characterized and applied in the pyrolysis of PE/PP mixture. The HUN-ZSM-5, Al-MCM-41(hhs), and Al-SBA-15(wo) were modified in house while the other common catalysts were prepared for comparison. Thermogravimetric studies on the decomposition of plastic feedstock showed that PE and PP shared a similar thermal behavior. However, the PE/PP mixture presented a slightly different thermal behavior from single PE and PP, implying interaction between PE and PP during pyrolysis. Both BET and XRD analyses of the six catalysts revealed the characteristic textural properties of the catalysts. NH_3-TPD analyses revealed that the acidity of the microporous catalysts was considerably stronger than that of the mesoporous catalysts. Microporous catalysts are known to produce great amounts of gas products with high selectivity of light aliphatic and aromatic compounds. This is caused by severe cracking of hydrocarbons due to the strong acidic nature of the catalyst. The modified catalyst, HUN-ZSM-5, exhibited a milder cracking activity and an exceptionally high selectivity for the gasoline fraction. On the other hand, catalytic pyrolysis with the mesoporous catalysts were characterized by lower yields of gaseous hydrocarbons and higher yields of liquid products rich in aliphatic compounds. Al-SBA-15(wo) showed the highest oil and wax yield among all the catalysts while Al-MCM-41(hhs) shared a similar product yield with KFS-16B, despite the fact that Al-MCM-41(hhs) possessed a higher BET surface area and greater number of strong acid sites. This indicated that the pyrolysis results over these catalysts were probably due to their characteristic acidity and textural property. The relationship between the characterizations of catalysts and the pyrolysis result was explored in depth, in order to provide further clues on the design and application of heterogeneous catalysts in solid waste treatment.

Acknowledgments: This research is funded by the National Environment Agency of Singapore under the Environment Technology Research Program (ETRP Grant No. 1202-109).

Author Contributions: Kaixin Li, Yanhui Yang, and Jing-Yuan Wang conceived and designed the experiments; Shao Wee Lee, Junxi Lei and Guoan Yuan performed the experiments; Kaixin Li and Guoan Yuan analyzed the data; Shengxuan Lin and Piyarat Weerachanchai contributed reagents/materials/analysis tools; Kaixin Li wrote the paper.

Conflicts of Interest: The authors declare no conflict of interest.

References

1. Keane, M.A. Catalytic transformation of waste polymers into fuel oil. *ChemSusChem* **2009**, *2*, 207–214. [CrossRef] [PubMed]
2. Gobin, K.; Manos, G. Polymer degradation to fuels over Microporous catalysts as a novel tertiary plastic recycling method. *Polym. Degrad. Stab.* **2004**, *83*, 267–279. [CrossRef]
3. Keane, M.A. Catalytic conversion of waste plastics: Focus on waste PVC. *J. Chem. Technol. Biotechnol.* **2007**, *82*, 787–795. [CrossRef]
4. Serrano, D.P.; Aguado, J.; Escola, J.M. Developing advanced catalysts for the conversion of polyolefinic waste plastics into fuels and chemicals. *ACS Catal.* **2012**, *2*, 1924–1941. [CrossRef]
5. Panda, A.K.; Singh, R.K.; Mishra, D.K. Thermolysis of waste plastics to liquid fuel: A suitable method for plastic waste management and manufacture of value added products—A world prospective. *Renew. Sust. Energy Rev.* **2010**, *14*, 233–248. [CrossRef]
6. Ivanova, S.R.; Gumerova, E.F.; Minsker, K.S.; Zaikov, G.E.; Berlin, A.A. Selective catalytic degradation of polyolefins. *Prog. Polym. Sci.* **1990**, *15*, 193–215. [CrossRef]
7. Adams, C.J.; Earle, M.J.; Seddon, K.R. Catalytic cracking reactions of polyethylene to light alkanes in ionic liquids. *Green Chem.* **2000**, *2*, 21–24. [CrossRef]
8. Satterfield, C.N. *Heterogeneous Catalysis in Industrial Practice*, 2nd ed.; Krieger Publishing: Malabar, FL, USA, 1996.
9. Aguado, J.; Serrano, D.P.; Van Grieken, R.; Escola, J.M.; Garagorri, E. 24-P-13-Catalytic properties of micelle templated Microporous and Mesoporous materials for the conversion of low-density polyethylene. *Stud. Surf. Sci. Catal.* **2001**, *135*, 273.
10. Garforth, A.; Fiddy, S.; Lin, Y.H.; Ghanbari-Siakhali, A.; Sharratt, P.; Dwyer, J. Catalytic degradation of high density polyethylene: an evaluation of mesoporous and microporous catalysts using thermal analysis. *Thermochim. Acta* **1997**, *294*, 65–69. [CrossRef]
11. Schirmer, J.; Kim, J.S.; Klemm, E. Catalytic degradation of polyethylene using thermal gravimetric analysis and a cycled-spheres-reactor. *J. Anal. Appl. Pyrolysis* **2001**, *60*, 205–217. [CrossRef]
12. Serrano, D.P.; Aguado, J.; Escola, J.; Rodríguez, J.; Morselli, L.; Orsi, R. Thermal and catalytic cracking of a LDPE–EVA copolymer mixture. *J. Anal. Appl. Pyrolysis* **2003**, *68*, 481–494. [CrossRef]
13. Serrano, D.P.; Aguado, J.; Escola, J.M.; Garagorri, E. Conversion of low density polyethylene into petrochemical feedstocks using a continuous screw kiln reactor. *J. Anal. Appl. Pyrolysis* **2001**, *58*, 789–801. [CrossRef]
14. Serrano, D.P.; Aguado, J.; Escola, J.M.; Garagorri, E.; Morselli, L.; Palazzi, G.; Orsi, R. Feedstock recycling of agriculture plastic film wastes by catalytic cracking. *Appl. Catal. B Environ.* **2004**, *49*, 257–265. [CrossRef]
15. Yusaku, S.; Azhar Uddin, M.; Akinori, M.; Yasufumi, K.; Kazuo, K.; Katsuhide, M. Catalytic degradation of polyethylene into fuel oil over mesoporous silica (KFS-16) catalyst. *J. Anal. Appl. Pyrolysis* **1997**, *43*, 15–25.
16. Renzinia, M.S.; Lerici, L.C.; Sedranb, U.; Pierella, L.B. Stability of ZSM-11 and BETA zeolites during the catalytic cracking of low-density polyethylene. *J. Anal. Appl. Pyrolysis* **2011**, *92*, 450–455. [CrossRef]
17. Bhangea, P.; Bhangea, D.S.; Pradhana, S.; Ramaswamy, V. Direct synthesis of well-ordered Mesoporous Al-SBA-15 and its correlation with the catalytic activity. *Appl. Catal. A Gen.* **2011**, *400*, 176–184. [CrossRef]
18. Song, C.M.; Jiang, J.; Yan, Z.F. Synthesis and characterization of MCM-41-type composite materials prepared from ZSM-5 zeolite. *J. Porous Mater.* **2008**, *15*, 205–211. [CrossRef]
19. Serrano, D.P.; Aguado, J.; Morales, G.; Rodriguez, J.M.; Peral, A.; Thommes, M.; Epping, J.D.; Chmelka, B.F. Molecular and meso-and macroscopic properties of hierarchical nanocrystalline ZSM-5 zeolite prepared by seed silanization. *Chem. Mater.* **2009**, *21*, 641–654. [CrossRef]
20. Hidalgo, C.V.; Itoh, H.; Hattori, T.; Niwa, M.; Murakami, Y. Measurement of the acidity of various zeolites by temperature-programmed desorption of ammonia. *J. Catal.* **1984**, *85*, 362–369. [CrossRef]

21. Resini, C.; Montanari, T.; Nappi, L.; Bagnasco, G.; Turco, M.; Busca, G.; Bregani, F.; Notaro, M.; Rocchini, G. Selective catalytic reduction of NO_x by methane over Co-H-MFI and Co-H-FER zeolite catalysts: characterisation and catalytic activity. *J. Catal.* **2003**, *214*, 179–190. [CrossRef]
22. Bockhorn, H.; Hornung, A.; Hornung, U.; Schawaller, D. Kinetic study on the thermal degradation of polypropylene and polyethylene. *J. Anal. Appl. Pyrolysis* **1999**, *48*, 93–109. [CrossRef]
23. López, A.; De Marco, I.; Caballero, B.M.; Laresgoiti, M.F.; Adrados, A.; Aranzabal, A. Catalytic pyrolysis of plastic wastes with two different types of catalysts: ZSM-5 zeolite and Red Mud. *Appl. Catal. B Environ.* **2011**, *104*, 211–219. [CrossRef]
24. Serrano, D.P.; Aguado, J.; Escola, J.M.; Rodríguez, J.M.; Peral, Á. Hierarchical zeolites with enhanced textural and catalytic properties synthesized from organofunctionalized seeds. *Chem. Mater.* **2006**, *18*, 2462–2464. [CrossRef]
25. Cesteros, Y.; Haller, G.L. Several factors affecting Al-MCM-41 synthesis. *Microporous Mesoporous Mater.* **2001**, *43*, 171–179. [CrossRef]
26. Aguado, J.; Serrano, D.P.; Escola, J.M. A sol–gel approach for the room temperature synthesis of Al-containing micelle-templated silica. *Microporous Mesoporous Mater.* **2000**, *34*, 43–54. [CrossRef]
27. Liu, W.-W.; Hu, C.-W.; Yang, Y.; Tong, D.-M.; Zhu, L.-F.; Zhang, R.-N.; Zhao, B.-H. Study on the effect of metal types in (Me)-Al-MCM-41 on the Mesoporous structure and catalytic behavior during the vapor-catalyzed co-pyrolysis of pubescens and LDPE. *Appl. Catal. B Environ.* **2013**, *129*, 202–213. [CrossRef]
28. Hernández, M.R.; Gómez, A.; García, Á.N.; Agulló, J.; Marcilla, A. Effect of the temperature in the nature and extension of the primary and secondary reactions in the thermal and HZSM-5 catalytic pyrolysis of HDPE. *Appl. Catal. A Gen.* **2007**, *317*, 183–194. [CrossRef]
29. Elordi, G.; Olazar, M.; Lopez, G.; Amutio, M.; Artetxe, M.; Aguado, R.; Bilbao, J. Catalytic pyrolysis of HDPE in continuous mode over zeolite catalysts in a conical spouted bed reactor. *J. Anal. Appl. Pyrolysis* **2009**, *85*, 345–351. [CrossRef]
30. González-Velasco, J.R.; López-Fonseca, R.; Aranzabal, A.; Gutiérrez-Ortiz, J.I.; Steltenpohl, P. Evaluation of H-type zeolites in the destructive oxidation of chlorinated volatile organic compounds. *Appl. Catal. B Environ.* **2000**, *24*, 233–242. [CrossRef]
31. Aguado, J.; Serrano, D.P.; San Miguel, G.; Escola, J.M.; Rodriguez, J.M. Catalytic activity of zeolitic and mesostructured catalysts in the cracking of pure and waste polyolefins. *J. Anal. Appl. Pyrolysis* **2007**, *78*, 153–161. [CrossRef]
32. Angyal, A.; Miskolczi, N.; Bartha, L.; Valkai, I. Catalytic cracking of polyethylene waste in horizontal tube reactor. *Polym. Degrad. Stab.* **2009**, *94*, 1678–1683. [CrossRef]
33. Mastral, J.F.; Berrueco, C.; Gea, M.; Ceamanos, J. Catalytic degradation of high density polyethylene over nanocrystalline HZSM-5 zeolite. *Polym. Degrad. Stab.* **2006**, *91*, 3330–3338. [CrossRef]
34. Aguado, J.; Serrano, D.P.; San Miguel, G.; Castro, M.C.; Madrid, S. Feedstock recycling of polyethylene in a two-step thermo-catalytic reaction system. *J. Anal. Appl. Pyrolysis* **2007**, *79*, 415–423. [CrossRef]
35. Chaianansutcharit, S.; Katsutath, R.; Chaisuwan, A.; Bhaskar, T.; Nigo, A.; Muto, A.; Sakata, Y. Catalytic degradation of polyolefins over hexagonal Mesoporous silica: Effect of aluminum addition. *J. Anal. Appl. Pyrolysis* **2007**, *80*, 360–368. [CrossRef]
36. Miskolczi, N.; Bartha, L.; Deák, G. Thermal degradation of polyethylene and polystyrene from the packaging industry over different catalysts into fuel-like feed stocks. *Polym. Degrad. Stab.* **2006**, *91*, 517–526. [CrossRef]
37. Marcilla, A.; Beltrán, M.; Navarro, R. Thermal and catalytic pyrolysis of polyethylene over HZSM5 and HUSY zeolites in a batch reactor under dynamic conditions. *Appl. Catal. B Environ.* **2009**, *86*, 78–86. [CrossRef]
38. Park, D.W.; Hwang, E.Y.; Kim, J.R.; Choi, J.K.; Kim, Y.A.; Woo, H.C. Catalytic degradation of polyethylene over solid acid catalysts. *Polym. Degrad. Stab.* **1999**, *65*, 193–198. [CrossRef]
39. Wei, T.T.; Wu, K.J.; Lee, S.L.; Lin, Y.H. Chemical recycling of post-consumer polymer waste over fluidizing cracking catalysts for producing chemicals and hydrocarbon fuels. *Resour. Conserv. Recycl.* **2010**, *54*, 952–961. [CrossRef]